AGU PUBLICATIONS

JGR

Journal of Geophysical Research: Space Physics

RESEARCH ARTICLE

10.1002/2017JA024087

Key Points:
- Measured 100 eV total emission cross section of the optically forbidden Lyman-Birge-Hopfield (LBH) band system of N_2 by electron-impact-induced fluorescence
- Laboratory experiment isolating single-scattering electron-impact-induced fluorescence from direct excitation and cascading contributions to the $a^1\Pi_g$ state of N_2
- Lifetime for the optically forbidden $a^1\Pi_g$ state is found to be ~50 ± 15 μs

Correspondence to:
J. M. Ajello,
joe.ajello@lasp.colorado.edu

Citation:
Ajello, J. M., C. P. Malone, G. M. Holsclaw, A. C. Hoskins, R. W. Eastes, W. E. McClintock, and P. V. Johnson (2017), Electron impact study of the 100 eV emission cross section and lifetime of the Lyman-Birge-Hopfield band system of N_2: Direct excitation and cascade, *J. Geophys. Res. Space Physics*, *122*, 6776-6790, doi:10.1002/2017JA024087.

Received 27 FEB 2017
Accepted 16 MAY 2017
Accepted article online 18 MAY 2017
Published online 21 JUN 2017

©2017. American Geophysical Union. All Rights Reserved.

Electron impact study of the 100 eV emission cross section and lifetime of the Lyman-Birge-Hopfield band system of N_2: Direct excitation and cascade

J. M. Ajello[1], C. P. Malone[2], G. M. Holsclaw[1], A. C. Hoskins[1], R. W. Eastes[3], W. E. McClintock[1], and P. V. Johnson[2]

[1]Laboratory for Atmospheric and Space Physics, University of Colorado Boulder, Boulder, Colorado, USA, [2]Jet Propulsion Laboratory, California Institute of Technology, Pasadena, California, USA, [3]Florida Space Institute, University of Central Florida, Orlando, Florida, USA

Abstract We have measured the 100 eV emission cross section of the optically forbidden Lyman-Birge-Hopfield (LBH) band system ($a^1\Pi_g \rightarrow X^1\Sigma_g^+$) of N_2 by electron-impact-induced fluorescence. Using a large (1.5 m diameter) vacuum chamber housing an electron gun system and the Mars Atmosphere and Volatile EvolutioN mission Imaging Ultraviolet Spectrograph optical engineering model, we have obtained calibrated spectral measurements of the LBH band system from 115 to 175 nm over a range of lines of sight to capture all of the optical emissions. These measurements represent the first experiment to directly isolate in the laboratory single-scattering electron-impact-induced fluorescence from both direct excitation of the $a^1\Pi_g$ state and cascading contributions to the $a^1\Pi_g$ state ($a'^1\Sigma_u^-$ and $w^1\Delta_u \rightarrow a^1\Pi_g \rightarrow X^1\Sigma_g^+$). The determination of the total LBH emission cross section is accomplished by measuring the entire cylindrical glow pattern of the metastable emission from electron impact by imaging lines of sight that measure the glow intensity from zero to ~400 mm radial distance and calculating the ratio of the integrated intensity from the LBH glow pattern to that of a simultaneously observed optically allowed transition with a well-established cross section: NI 120.0 nm. The "direct" emission cross section of the $a^1\Pi_g$ state at 100 eV was determined to be $\sigma_{\mathrm{dir}}^{\mathrm{em}} = (6.41 \pm 1.3) \times 10^{-18}$ cm^2. An important observation from the glow pattern behavior is that the total (direct + cascading) emission cross section is pressure dependent due to collision-induced cascade transitions between close-lying electronic states.

1. Introduction

The ultraviolet (UV) emissions from the Earth's thermosphere play a key role in our current capabilities for remotely sensing the Earth's space environment (SE) [*Meier et al.*, 2015; *Paxton et al.*, 1999]. The aeronomy community has identified the Lyman-Birge-Hopfield (LBH) band system of molecular nitrogen ($a^1\Pi_g \rightarrow X^1\Sigma_g^+$) as the key atmospheric emission to be observed by satellites for monitoring the global energy input into geospace [*Kanik et al.*, 2000; *Aksnes et al.*, 2006, 2007; *Kil et al.*, 2011; *Krywonos et al.*, 2012] with an anticipated measurement accuracy of 5–10%. However, anomalies in understanding the vibrational distribution and band intensities of the N_2 LBH band system have brought into question the reliability of such monitoring by our spacecraft [*Eastes et al.*, 2008; *Eastes and Dentamaro*, 1996; *Eastes*, 2000]. Recent space missions, with UV detectors on board, measuring the LBH emissions for SE determination (e.g., atmospheric temperature and O/N_2 density ratio) have been summarized [*Eastes et al.*, 2011; *Ajello et al.*, 2011a; *Young et al.*, 2010]. These LBH band emission observing satellites include the Thermosphere Ionosphere Mesosphere Energetics and Dynamics satellite with the Global Ultraviolet Imager, the Midcourse Space Experiment with multispectral capability from the far ultraviolet (FUV) to the infrared (IR) of the Ballistic Missile Defense Organization, the UV imager on the Polar spacecraft of the Global Geospace Science portion of the International Solar Terrestrial Physics program, the Imager for Magnetopause-to-Aurora Global Exploration satellite, and the Defense Meteorological Satellite Program, the latter being a series of spacecraft with two UV instruments: Special Sensor Ultraviolet Limb Imager and Special Sensor Ultraviolet Spectrographic Imager [*Meier et al.*, 2005; *Vanhamäki and Amm*, 2011].

The planned 2017 launches of the GOLD (Global-scale Observations of the Limb and Disk) and Ionospheric Connection Explorer satellites will provide solar cycle 24 data on the physical connection between Earth and the immediate SE as well as temperatures in Earth's thermosphere and ionosphere

[*Eastes et al.*, 2008, 2011, 2015; *Mannucci et al.*, 2012]. GOLD will conduct simultaneous dayglow LBH and atomic oxygen UV measurements to determine temperature and composition in the thermosphere-ionosphere system on a global scale. The accuracy with which thermospheric neutral composition and temperature can be determined from such observations depends upon the accuracy of the model used, which itself is dependent on the accuracy of the excitation and emission cross sections available for O and N_2.

Our laboratory work, described in this paper and performed at the University of Colorado (CU), improves the accuracy of the relevant cross sections for N_2. We have been able to show that the total LBH emission ($a^1\Pi_g \rightarrow X^1\Sigma_g^+$) is generated by two equally important processes: (i) direct excitation ($X^1\Sigma_g^+ \rightarrow a^1\Pi_g$) resulting in optically forbidden fluorescence by magnetic dipole and electric quadrupole moments and (ii) indirect excitation of the *a* state via dipole-allowed radiative and collisional-induced electronic transition (CIET) cascade processes (i.e., $a'^1\Sigma_u^- \rightarrow a^1\Pi_g$ and $w^1\Delta_u \rightarrow a^1\Pi_g$) [*Eastes and Dentamaro*, 1996; *Malone et al.*, 2015]. Note that "fast" cascade population of the *a* state can occur from the $c_4'^1\Sigma_u^+$ state and similar upper Rydberg-valence states, but it has been shown to apparently be insignificant (<1% branching [see *Filippelli et al.*, 1984; *Allen and Lin*, 1989; *Allen et al.*, 1990; *Shemansky et al.*, 1995]). Cascading processes result in a large increase in the LBH emission intensity at electron collision energies of 10–100 eV, which also corresponds to the typical energy range for secondary electrons in the upper atmosphere. Modeling can now more accurately include excitation by cascade, in addition to direct excitation, for determination of composition and temperature in the SE, as well as the flow of solar energy through geospace from electron transport models. However, the cross section for cascading is expected to be pressure-dependent [*Eastes and Dentamaro*, 1996]. This cross-section variation with pressure and energy must be measured for input into electron transport models for dayglow and auroral analysis [*Lummerzheim and Galand*, 2001]. We make the first step here in a laboratory experiment at 100 eV (corresponding to a standard energy, having commonality with many previous measurements) conducted at an atmospheric pressure representative of an altitude of ~120–130 km on Earth, which is near the peak altitude of the LBH dayglow emission region [see *Eastes and Dentamaro*, 1996, Table 4].

We have successfully modified a large vacuum system apparatus normally used for optical calibration of flight instruments [see, e.g., *McClintock et al.*, 2015] into an apparatus for measuring the emission cross sections of two of the strongest transitions and optically forbidden transitions found in the Earth's airglow: the LBH bands and OI 135.6 nm. The experimental instrumentation prepared at CU is currently using the Mars Atmosphere and Volatile EvolutioN (MAVEN) mission Imaging Ultraviolet Spectrograph (IUVS) optical engineering model (nearly identical to the flight instrument) to observe the glow pattern of electron-impact-induced fluorescence of metastable transitions. This laboratory instrumentation allows us to obtain in a single observation a wide-angle (11.3°) image of the radial extent of the emissions, capturing both the metastable and allowed transitions occurring in the FUV (from 115 to 190 nm) and middle-ultraviolet (MUV; from 180 to 330 nm) from particle impact on N_2, O_2, CO, and CO_2 [*McClintock et al.*, 2015; *Malone et al.*, 2015; *Ajello et al.*, 2011b; *Kanik et al.*, 2003]. Only the work on N_2 is reported here.

The N_2 radial glow pattern is composed of apparently two distinct emissions with different behaviors with respect to distance from the electron beam. In this paper we compare the radial intensity variation of the dipole-allowed NI 120.0 nm multiplet ($^4P \rightarrow {}^4S^o$) and the LBH band system with respect to distance from the electron beam. The change in slope of the LBH glow intensity pattern with respect to radius allows separation of the shorter-lived direct emission from the longer-lived cascade emissions. The lifetime for direct emission has been reported by *Marinelli et al.* [1989], who find the lifetime to be 56 ± 4 μs for $v' = 0$–2. This is consistent with the theoretical predictions of *Dahl and Oddershede* [1986] and the experimental upper limit of 80 μs determined by *Holland* [1969]. The spectroscopic data of *Laher and Gilmore* [1991], *Gilmore et al.* [1992], and *Laher* [1999] suggest lifetimes near 58–61 μs for $v' = 0$–3 (with additional v'-levels tabulated). *Kedzierski and McConkey* [2016a, 2016b] also just published work on N_2 that included an estimate of the LBH lifetime of ~75 μs; their measurement was capable of including some undetermined portion of "slow" cascade.

The LBH lifetime greatly affects the size of the glow region and thus changes the estimate of the percentage of the glow region observed in the static gas detector experiments studied here. The earlier glow profiles [*Ajello*, 1970; *Ajello and Shemansky*, 1985] were calculated using the 80 μs lifetime of Holland, an upper limit that did not consider cascading. Therefore, an independent check of the lifetime of this state from our experiment that can resolve direct excitation and cascade lifetimes is worthwhile. The lifetime measurements of *Marinelli et al.* [1989] used laser excitation and effectively eliminated radiative and collisional cascade to

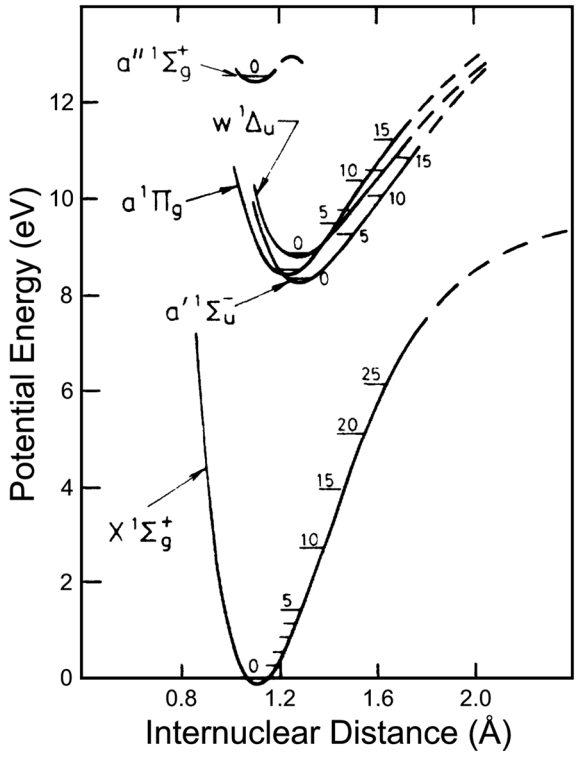

Figure 1. Partial energy level diagram of lower electronic states of N_2 (adapted from *Brunger and Teubner* [1990]).

the *a* state. There is marked difference between the *a*′-state and *w*-state lifetimes to the ground state. The *a*′-state lifetime by *Wilkinson and Mulliken* [1959] is found to be ~40 ms, while *Tilford and Benesch* [1976] find the lifetime to be ~13 ms for $v' = 0$, noting that $a'(0)$ resides below $a(0)$. More recently, *Eastes and Dentamaro* [1996] recommend a lifetime for the *a*′ state of ~17 ms to the ground state. The *w* state is radiatively decoupled from the ground state and can only be depopulated by CIET. We thus note that the $a'^1\Sigma_u^-$ and $w^1\Delta_u$ states have long radiative lifetimes to the ground state, roughly 13–40 ms [*Casassa and Golde*, 1979; *Tilford and Benesch*, 1976] for the $a'^1\Sigma_u^- \rightarrow X^1\Sigma_g^+$ forbidden transition (that proceeds through nearby $^1\Pi_u$ states) and at least seconds for the forbidden $w^1\Delta_u \rightarrow X^1\Sigma_g^+$ transition, with additional "direct emission" $a'^1\Sigma_u^- \rightarrow a^1\Pi_g$ and $w^1\Delta_u \rightarrow a^1\Pi_g$ fluorescence between 3000 and 8500 nm (3.0 and 8.5 μm) in the IR, named the McFarlane I and II bands, respectively. Their radiative cascade effect to the LBH band system emission intensity has never been measured by single-scattering e^- + N_2-induced fluorescence [*Lofthus and Krupenie*, 1977; *Itikawa et al.*, 1986; *Itikawa*, 2006]. Their radiative IR fluorescence is expected to be small due to the low frequency of these transitions; i.e., the energy gap between the states is small (Figure 1) [*Brunger and Teubner*, 1990].

Previously, *Meier* [1991] and *Ajello et al.* [2011a] have reviewed the combined effect of N_2^* cascades from the $a'^1\Sigma_u^-$ and $w^1\Delta_u$ states by electron impact using the results of *Cartwright* [1978] and showed that their contribution to the LBH emission can be significant (>25%). It should be noted that the excitation cross sections used by *Cartwright* [1978] are based on the integral cross sections of *Cartwright et al.* [1977b], which are based on the underlying energy-loss-derived differential cross sections of *Cartwright et al.* [1977a], and are largely estimated interpolations (and extrapolations) of sparse experimental data points that depended on assumed Franck-Condon (FC) behavior even near to threshold (note that FC behavior has been shown to deviate at lower impact energies [see *Khakoo et al.*, 2008; *Malone et al.*, 2009a, 2009b, 2009c, 2012]). Consequently, the results of *Cartwright* [1978] should be used with caution. We also note that *Eastes and Dentamaro* [1996] have shown that the rate for CIET for $a' \leftrightarrow a$ and $w \leftrightarrow a$ is significant at the altitudes for LBH emissions from Earth's atmosphere. CIET and radiative cascade lead to LBH vibrational distributions that are different from Franck-Condon vibrational distributions; radiative cascade by itself enhances the lower vibrational levels. *Cartwright* [1978] (via *Cartwright et al.* [1977b]) and *Johnson et al.* [2005] have shown that the total cross section of the optically forbidden excitation of the *a*′ and *w* states are roughly 28% of the *a* state near 20 eV; the coupling of these states by CIET calculated by *Eastes and Dentamaro* [1996] could further alter the *a*-state LBH emission. With the new results for cascading effects presented here we can finally assert that for the first time there may be better agreement in atmospheric modeling and satellite experiment for the LBH bands by forward and backward (multilinear regression) radiative transfer modeling—a significant result [*Stevens et al.*, 2015].

The main source of uncertainty in forward modeling radiative transport codes like Atmospheric Ultraviolet Radiance Integrated Code (AURIC) is the uncertainty in the magnitude of the cascade contributions

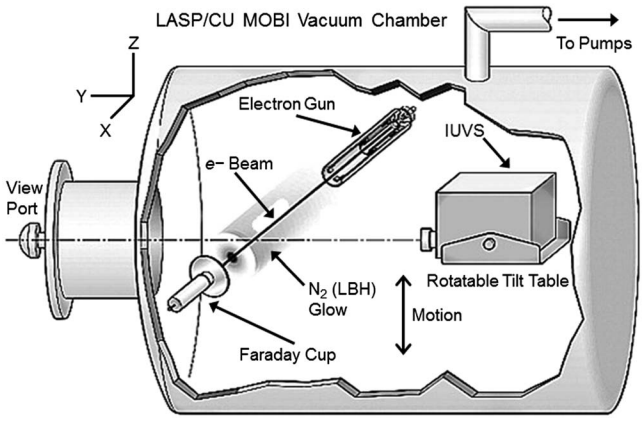

Figure 2. Schematic of the N_2 LBH glow experiment with the MAVEN IUVS using a 0.3 m electrostatic electron gun.

[*Strickland et al.*, 1999; *Knight et al.*, 2008]. The published variations in the magnitude of emission cross sections could be due to experimental limitations in fully capturing the long-lived emitting states, improper accounting of cascade contributions, or both. For instance, published σ^{em} data measured in a small collision chamber, compared to the much larger one in this paper, might have failed to account for the long-lived states diffusing outside the instrument detection field-of-view (FOV) (see *Filippelli et al.* [1994] for detailed discussion). Thus slow cascade from the long-lived $a'^1\Sigma_u^-$ and $w^1\Delta_u$ states to the $a^1\Pi_g$ state would be poorly constrained without these laboratory measurements.

2. Experimental Apparatus

The experimental apparatus for emission cross sections has been discussed in detail previously [*Noren et al.*, 2001; *Kanik et al.*, 2003]. We have previously published the work on OI (135.6 nm) from dissociation of O_2 using the Cassini UVIS (Ultraviolet Imaging Spectrograph) [*Kanik et al.*, 2003; *Makarov et al.*, 2003]. Similarly, the experiment reported here passed an electron beam through a static nitrogen gas and measured the glow profile produced around the electron beam. Ideally, an infinitely long electron beam will produce a cylindrically uniform glow region, where the emission and excitation rates per unit length of the beam are equal. We can approximate this condition by making the chamber large and the electron beam as long as possible such that edge effects are negligible [see, e.g., *Ajello*, 1970; *Holland*, 1969; *Filippelli et al.*, 1994].

A large chamber at CU, referred to as the Multi-Optical Beam Instrument (MOBI), is large enough to meet this condition with its 1.5 m diameter girth and 2.35 m length. The experimental apparatus, installed in the MOBI chamber, consisted of an electrostatic electron gun, Faraday cup, two pair of Helmholtz coils, a gas source, and the optical engineering model of the MAVEN IUVS instrument. Figure 2 schematically shows the MOBI vacuum chamber and IUVS observation geometry of the electron beam. The IUVS was mounted on a four-axis programmable motion platform inside the vacuum chamber that allowed *x* and *z* translation, as well as rotation in the *x*-*y* plane. The vacuum chamber had a base pressure of ~6.6×10^{-7} torr that was monitored by using an ionization gauge and inverted magnetron and was pumped by a large ADP Cryogenics Inc. cryopump. A turbo pump was also available to assist pumping when using H_2 during calibration.

The IUVS instrument is an imaging spectrograph with both FUV and MUV imaging channels. The two-dimensional imaging detectors (1024 spatial pixels and 1024 spectral pixels) for the optical channel are identical except that the input photocathode and window are CsI and MgF_2 for the FUV channel and CsTe with fused silica for the MUV channel. The FOV of the IUVS telescope is 11.3° × 0.06°, providing a large angular FOV of the glow region with the entrance slit of the spectrograph mounted perpendicular to the electron beam. This instrument was better suited for studying the spatially extended glow of metastable LBH emissions of the present paper compared to the Cassini UVIS used previously for OI (135.6 nm), which has a FOV in the FUV of only 60 mR × 1.5 mR (~3° × ~0.1°) [*Esposito et al.*, 2004; *Ajello et al.*, 2007, 2008; *Kanik et al.*, 2003].

The IUVS measures two types of spectral images over the full complement of 1024 spatial pixels: first, a high spectral resolution (0.6 nm full width at half maximum (FWHM)) narrow slit range of spatial pixels (79–913) in the center part of the slit and, second, a lower spectral resolution (2.5 nm FWHM) broad occultation-slit range of spatial pixels (0–78) and (914–1023) at the top and bottom of the slit, which are normally used only for stellar occultation observations. We used 835 spatial pixels in each image. Each 1024 × 1024 pixel-array detector measures photons over an active area of 24 mm^2, which gives a narrow pixel dimension of ~0.0235 mm for

pixels located at the center of the slit away from the two occultation-slit portions. Since the IUVS is designed to image objects at infinity, a shim was added to the telescope mirror to move the object plane to the electron beam ~41 inches (104.1 cm) from the instrument and to place the slit at the image plane located at 110.6 mm from the 100 mm focal length telescope mirror. The resulting image of the beam on the slit plane had a magnification for this experiment of $M = s/s' = 9.41$, where s is the object distance and s' is the image distance. The IUVS is a Czerny-Turner spectrograph design and images the entrance slit with unity magnification on the image-intensifier detectors using a spherical collimator, planar grating, and a toroidal focusing mirror to limit astigmatism. The slit at the focal plane is 0.1 mm wide by 19.8 mm high and is imaged on the detector with a resolution of 0.6 nm FWHM (full width at half maximum) in the FUV with a dispersion of 3.64 nm/mm [*McClintock et al.*, 2015]. Each spatial pixel views an object height in the glow region of 9.41×0.0235 mm = 0.221 mm (221 μm) perpendicular to the electron beam. The total vertical FOV for the 835 spatial pixels is ~7.3 inches (185 mm) for each image position. Our analysis consisted of sets of individual spectra summed over 10 spatial pixels and each average spatial data point represents 2.21 mm in object space (radius about the beam).

In the present work, the IUVS instrument was placed on a vertical moving stage with the entrance slit orthogonal to the electron beam. With staged three-step motion, this FOV was expanded to more than 400 mm from the electron beam allowing the observation from metastable emissions. Three images were taken at different stage positions to capture the glow region from long-lived states such as N_2 (LBH). We can vary the vertical height of the placement of the optic axis of the IUVS at three positions above the electron beam axis. We start from Image 1 on the center ($z = 0$) with the emission from allowed transitions centered near spatial pixel 500, followed by a motion in the z direction to obtain Image 2 centered at 16 cm, and Image 3 centered at 32 cm above the electron beam.

The design of the electrostatic electron gun has been previously described by *Makarov et al.* [2003] and *Kanik et al.* [2003] and is described in *Harting and Read* [1976]. In brief, the electron gun consisted of a large focal length (0.3 m) with electrostatic focusing along with Helmholtz coils wrapped on the outside of the MOBI chamber to maintain the straight path on the electron gun center line without significant curvature from Earth's ~0.5 G magnetic field. The electron gun was constructed from the two-cylinder (ratio of diameters is two) lens design of *Harting and Read* [1976] such that the lens voltages can be set to establish a 30 cm focal length with 20 μA beam current at 30 eV. In the present setup, an electron beam with an energy of 100 eV (chosen due to it being a standard energy with many measurements) can be deflected by the Earth's magnetic field approximately 15 cm from its intended path without the coils. A gaussmeter was used to zero the magnetic field at the electron beam center, and the multielement Faraday cup was used to optimize the electron beam current. A viewport was used to observe the glow region with a blue emission emanating as a visibly straight line along the electron beam from dipole-allowed N_2^+ 391.4 nm emission. The straight-line appearance of the ~30 cm long electron beam ensures correct voltage settings of the two pairs of Helmholtz coils set to eliminate curvature of the electron beam from the Earth's magnetic field. The electron beam collected Faraday cup current is nominally ~300 μA (though set to ~10–400 μA depending on requirements) with some scattering of current going to a large (30.5 cm radius) plate at the entrance aperture to the Faraday cup. In this experiment for N_2 at 100 eV, only ~2.3 μA went to the plate while the Faraday cup collected ~292 μA.

The axially symmetric glow of emitted photons, resulting from a radiative decay of the excited NI and N_2 states, was detected at 90° with respect to the boresight of the IUVS. The gas pressure range was maintained in the molecular flow regime during the measurements (1.5×10^{-5} torr) as the trapping of resonance radiation can reduce the detected emission significantly at high gas pressure. For the LBH bands studied, this was not a concern since the molecular bands do not arise from a dipole-allowed transition [see *Filippelli et al.*, 1984; *Young et al.*, 2010]; polarization of the fluorescence was also negligible. For the NI 120.0 nm multiplet ($^4P \rightarrow {}^4S^o$), resonance absorption could be a factor, but since the atomic N is created from dissociation of N_2, the quantity of N in the FOV was negligible. We use the standard NI 120.0 nm emission cross section at 100 eV from N_2 to be $(3.7 \pm 0.5) \times 10^{-18}$ cm^2 [*Malone et al.*, 2008] for determining the LBH cross section.

The 100 eV emission data presented here were collected with an electron beam current of ~292 μA and a gas pressure of $\sim 1.5 \times 10^{-5}$ torr. It is noteworthy that the gas pressure is equivalent to a number density of $\sim 5.4 \times 10^{11}$ cm^{-3}, which is the same N_2 density as found near 120–130 km on Earth [*Eastes and*

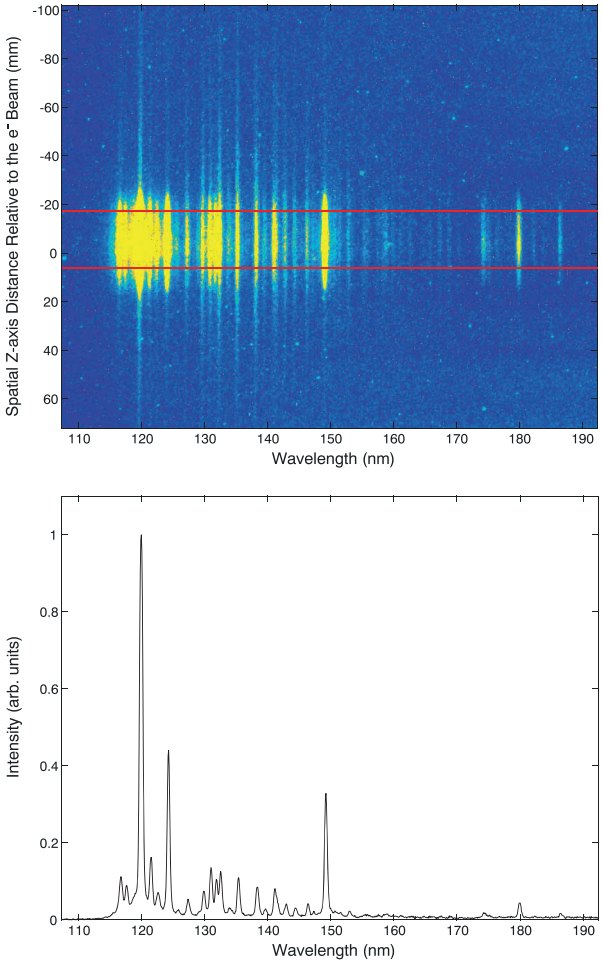

Figure 3. The Image 1 view of our file "N2_100eV_4" showing 1024 × 835 pixels. This spatial-pixel summed FUV spectrum makes use of spatial channels numbered from 79 to 913. The composite FUV spectrum required 80 min for eight loops with eight images of bright signal per loop with a time of 1 min per bright image. The bright column of pixels occurs for the allowed transitions occurring on the electron beam. The red boundary lines indicate the NI 120.0 nm glow FWHM (see Figure 7 and text following equation (4)). The straight-line signal verifies that the Helmholtz coils have accurately compensated for the Earth's magnetic field by steering the electron beam.

Dentamaro, 1996]. CIET rate contributions to the *a*-state emission from $a' \leftrightarrow a$ and $w \leftrightarrow a$ coupling at this density are found to be significant, enhancing the radiation by a factor of ~2–3 from a case of low-density collisionless emissions without CIET [see *Eastes and Dentamaro*, 1996, Table 4; *Eastes*, 2000]. Note that the intensity enhancement is strongest for low vibrational levels (i.e., $v' < 3$) of the *a* state.

3. Laboratory Measurements of LBH Bands

We show in Figure 3 the spatial-spectral image obtained by the IUVS for Image 1 on-center geometry. MOBI was filled with a static gas sample of N_2 at 1.5×10^{-5} torr (5.4×10^{11} cm^{-3}), and the electron gun provided an electron beam current of ~292 μA. The FUV spectrum of 1024 spectral pixels was obtained in second order yielding about 0.08 nm per channel with a resolution of 0.6 nm FWHM. The raw and uncalibrated FUV spectrum in the lower half of Figure 3 is the spatial pixel-summed composite of eight images per cycle of about 65 s each per image with 5 s time allotted for readout of the detector to mitigate pileup after each 60 s of exposure time. The imaging measurement represents about 1 h of data observation time with each cycle duration of approximately 10 min, since there are an additional two loops at the beginning and end of the set of eight images, which are important for measuring the background. The background was obtained by reducing the microchannel-plated detector high voltage from 900 V to 70 V.

We show the relative sensitivity calibration curve with wavelength in Figure 4. The relative sensitivity calibration data were obtained by measuring the intensities of emissions from electron impact fluorescence of both molecular hydrogen and molecular nitrogen in the 110–170 nm range and comparing them in each case to the modeled H_2 and N_2 intensities [*Ajello et al.*, 1988, 2002; *Liu et al.*, 1995]. The resulting FUV calibration of the "flight-spare" optical-engineering IUVS is shown in Figure 4 with a fourth-degree polynomial fit for the two molecular-branching ratio experiments along with a comparison to the flight IUVS sensitivity. Peak sensitivity for both instruments occurs around 125–130 nm (in second order) based on the CsI peak quantum efficiency and blaze-wavelength of the gratings at 280 nm in first order.

The electron-impact-induced fluorescence FUV spectrum shown in Figure 3 can be calibrated based on Figure 4, with the calibrated FUV spectrum shown in Figure 5. We add row pixels from columns that do not include the two large occultation apertures placed near the ends of the slit as described previously [see *McClintock et al.*, 2015].

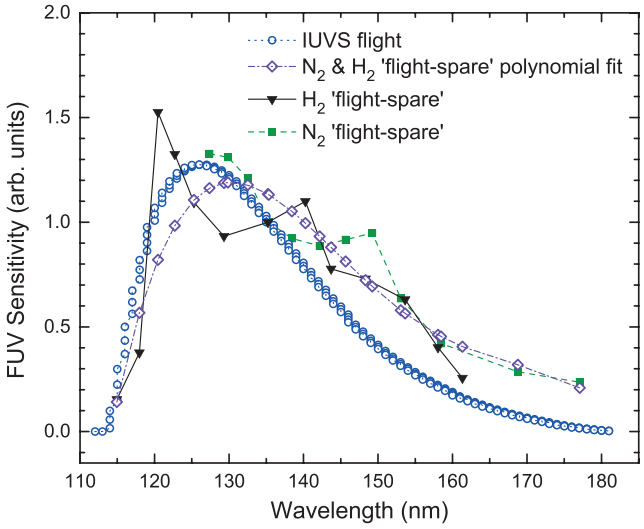

Figure 4. The FUV sensitivity of the MAVEN flight spare breadboard IUVS as a function of wavelength by two molecular branching ratio techniques described in *Ajello et al.* [1989, 2001] and *Liu et al.* [1995]. Based on Liu et al., we show in black the FUV sensitivity based on a model of the H_2 Lyman bands. Based on *Ajello et al.* [1988], we show in green the FUV sensitivity based on a model of the LBH bands. The composite mean sensitivity as a fourth-degree polynomial is shown in purple from 115 nm to 175 nm. The flight spectrometer sensitivity from *McClintock et al.* [2015] is shown in blue.

In the vacuum UV, we find that molecular emission was observed from a single electronic state of N_2 to the ground state. Fluorescence of the electronically lower lying metastable $a^1\Pi_g$ state of N_2 is known to depend on cascading from the $a'^1\Sigma_u^-$ and $w^1\Delta_u$ singlet electronic states with overlapping vibrational levels shown in Figure 1 [*Eastes and Dentamaro*, 1996; *Eastes*, 2000; *Young et al.*, 2010]. We take advantage of the fact that the wavelength range of 133.5–140.0 nm contains only LBH bands representing ~14% of the band system without any contamination from atomic N multiplets and use the integrated intensities (i.e., intensities summed over positive z translation above the electron beam from 0–400 mm) from this portion of the LBH band system to deduce the cross section of the band system [*Ajello and Shemansky*, 1985]. We determine from glow models that we were able to measure >98% of the emitted photons in the 133.5–140.0 nm spectral interval that arise from direct excitation. The two strongest bands of the LBH system dominate this spectral range: the (2,0) and (5,3) bands at 138.3 nm and the (3,0) and (6,2) bands at 135.3 nm. In addition, we included in this interval the (5,1) band at 133.9 nm and the (6,3) and (3,1) bands at 139.5 nm.

We show the radial glow pattern of the LBH bands and NI 120.0 nm for combined Images 1, 2, and 3 in Figure 6. Two of the images (2 and 3) are off-centered from the electron beam axis at minimum-ray height distances of 160 mm and 320 mm above the electron beam axis at 0 mm (Image 1). The radial glow pattern extends from beam center at 0 mm to 400 mm. The NI 120.0 nm ($^4P \rightarrow {}^4S^o$) signal, with a lifetime of ~1 ns and

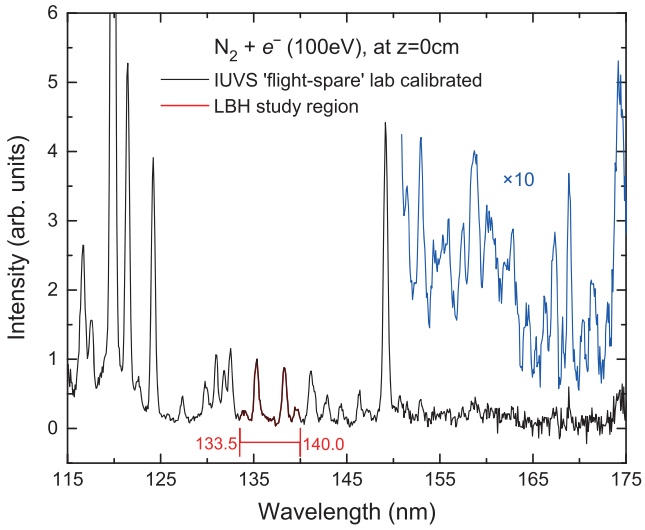

Figure 5. Calibrated Image 1 (z = 0) FUV electron-impact-induced fluorescence spectrum of N_2 between 115 and 175 nm for 100 eV electron-impact collision energy. A range of LBH molecular emission bands for this study between 133.5 and 140.0 nm is labeled. The x10 data inset was boxcar smoothed for display.

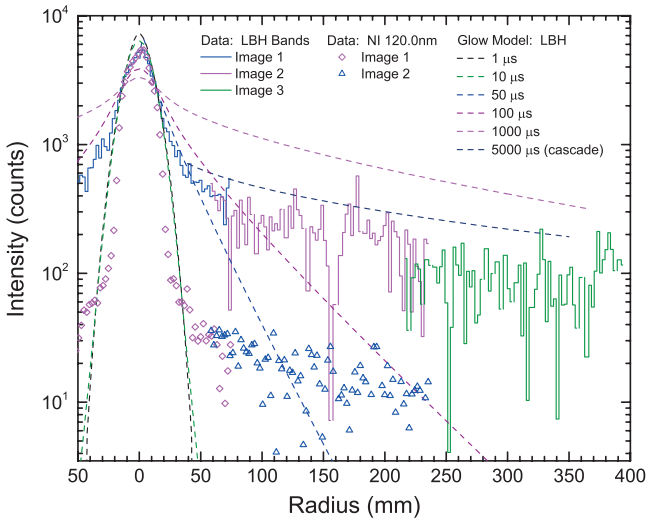

Figure 6. The glow pattern of NI 120.0 nm and LBH bands between 133.5 and 140.0 nm representing about 14% of the LBH band system but completely clear of atomic N features. This radial glow pattern extends from beam center at 0 mm to 400 mm and is the overlapping image of Images 1–3 with optic axis of the IUVS centered at 0, 16, and 32 cm from the electron beam axis at 0 cm (see Figure 2; motion below $z = 0$ is shown as a positive radius to the left of the origin). Included in the figure are modeled glow patterns as a function of lifetime from 1 μs to 1000 μs for direct excitation of the $a^1\Pi_g$ state and one model at 5000 μs for slow cascade to the $a^1\Pi_g$ state.

minor contributions from optically forbidden cascading, drops by 3 orders of magnitude and the LBH signal drops by 2 orders of magnitude. Even the NI 120.0 nm multiplet emission has a small cascading component from metastable upper states that contributes to a glow at large radii or the signal at large radii could be due to the ~1% of scattered electrons measured at the Faraday cup outer plate.

Figure 6 shows the normalized line-of-sight integrated emission intensities for the N_2 (LBH) and NI (120.0 nm) features, respectively, as a function of minimum-ray height (radius) from the electron beam. The radial glow pattern can be fit using two distinct types of emission processes with distance from the electron beam as shown in Figure 6. The change in slope (intensity versus radius) of the glow pattern at about 40 mm radial distance allows separation of the direct and longer-lived cascade emissions. This change in slope occurs based on the different lifetimes of the two types of LBH emission processes as described below.

1. Directly populated $a^1\Pi_g$:

$$e^- + N_2\ (X) \rightarrow N_2^*\ (a) \rightarrow e^- + N_2\ (X) + h\nu\ (\mathrm{LBH}).$$

2. Indirectly populated $a^1\Pi_g$ via slow IR-cascade and CIET from the a' and w states (whose individual lifetimes >1 ms):

$$e^- + N_2\ (X) \rightarrow N_2^{**} \rightarrow e^- + N_2\ (X) + h\nu\ (\mathrm{LBH}).$$

Shown for comparison with the measurement of LBH intensity versus radius are an array of glow patterns from direct excitation for five different lifetimes from 1 to 1000 μs. The experimental area under each experimental curve for the LBH band system and NI 120.0 nm multiplet was integrated with respect to linear displacement in the z direction (i.e., with radius) to obtain the total emission intensity for each of the features being studied to a radius of 400 mm.

The electron-induced fluorescence volume emission rate, $I_{v'v''}(r)$, from any LBH vibrational band (v',v'') of the $a^1\Pi_g$ state as a function of radius r (about the electron beam with current J for a gas density of N_o at 300 K with mean gas velocity v_m) is approximately [*Ajello*, 1970; *Holland*, 1969; *Filippelli et al.*, 1994] given by

$$I_{v'v''}\ (r) \sim N_o\ \sigma_{v'v''}\ (J/e)\ \exp[-r/(\tau\ v_m)]/(r\ \tau\ v_m), \quad (1)$$

where $r = (y^2 + z^2)^{1/2}$ (see Figure 2), τ is the lifetime of the $a^1\Pi_g$ state from direct excitation, and $\sigma_{v'v''}$ is the emission cross section of the vibrational band (v',v''). We use equation (1) to calculate the LBH glow signal in equation (2) as a function of minimum ray height radius to the line of sight. The LBH volume emission

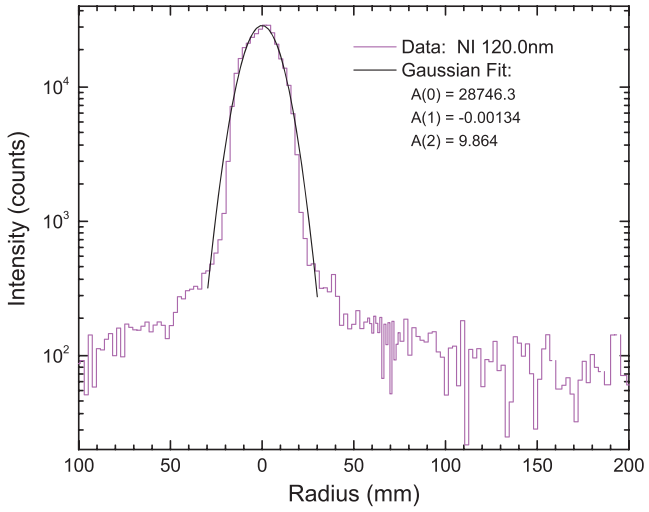

Figure 7. A mathematical Gaussian fit to the NI 120.0 nm glow data as a function of radial distance, *z*, with constants for three-dimensional vector A given in the figure. The GAUSS fit function (in IDL) computes a nonlinear least squares fit (referred to as *Int*) to the NI 120.0 nm intensity points in Figure 6 with three unknown vectors: A[0], A[1], and A[2] given in the figure.

rate falls off a little faster than r^{-1} due to the exponential factor with lifetime. A similar expression like equation (1) can be attributed to cascading with a second lifetime τ_{casc}. One case for a radial glow shows a sample direct lifetime of 35 μs, with a second lifetime component of ~5 ms dominating beyond 40 mm, as indicated in Figure 6.

The total estimated signal in counts/s from the more spatially extended N_2 (LBH) glow pattern at any position *y*, along the IUVS line of sight (see Figure 2), is proportional to the integral of the line-of-sight column emission intensity through the glow region. These lines of sight must be summed with respect to the linear displacement *z* of the line of sight (minimum-ray height radius of glow region) of the IUVS from the starting position of the electron beam at $z = 0$. The total LBH signal in counts per second at a particular wavelength from the entire chamber is a double integral:

$$\text{Sig (LBH)} = \varepsilon_{\text{LBH}}\, A_{\text{mir}}\, K_{\text{geom}} \iint 4\pi\, I_{\text{LBH}}\,(y,z)\, dy\, dz, \tag{2}$$

where A_{mir} is the area of the telescope mirror; $4\pi\, I_{\text{LBH}}$ is the integrated intensity (photons $\text{cm}^{-2}\,\text{s}^{-1}$) along line of sight, *y*, with minimum ray height of the column pixel FOV displaced *z* from the electron beam; K_{geom} is a geometry factor of the glow region examined by the IUVS FOV (11.3° × 0.06°) at a distance of 104.1 cm from IUVS; and ε_{LBH} is the mean efficiency of the optical system in counts per photon at, for example, 135.6 nm, the mean wavelength of the LBH spectral interval (133.0–139.5 nm). The measured LBH signal in equation (2) at any line-of-sight height (*z*) above the electron beam is a line-of-sight integral dependent on the volume emission rate, $I_{\text{LBH}}(y,z)$.

The relative sensitivity in Figure 4 varies by less than 18% over this interval from 1.18 at 132.5 nm to 1.00 at 140.0 nm. Essentially, all the directly excited *a*-state molecules are being observed with our measured lifetime of 50 μs (to be described later and shown in Figure 6) for the *a* state. The distance that an excited LBH molecule travels before spontaneous emission occurs at the mean thermal energy of 38.8 MeV at 300 K is only ~26 mm. Since the LBH line-of-sight emission intensity, defined in the integrand of equation (1), with respect to *z*, is proportional to the volume emission rate, the LBH emission cross section for direct excitation can be found. The distance an a'-excited molecule will travel depends on its lifetime. This distance is 257 cm for a combined CIET + radiative mean lifetime of 5 ms (this work) or nearly 1 m for the radiative lifetime of 17 ms to the ground *X* state for a collisionless regime [*Casassa and Golde*, 1979]. The *w* state is dipole-allowed to radiatively couple to the *a* state and may be the cause at 100 eV of the extended glow region. It may not be possible to measure all the cascade emission at this gas pressure, and we only provide a lower limit in this study because when CIET is important the *a*-state emission cross section for aeronomy is pressure-dependent.

We show a mathematical Gaussian fit to the NI 120.0 nm glow data as a function of radial distance (column position on the image), *z*, with constants for three-dimensional vector "A" given in Figure 7. The GAUSSFIT function (of Interactive Data Language (IDL)) computes a nonlinear least squares fit, "*Int*," to the NI 120.0 nm intensity points (10 IUVS column pixels per point) in Figure 6 with three unknown scalar values for vector A: A[0], A[1], and A[2] are given in equations (3) and (4).

$$B = (z - \text{A}[1])/\text{A}[2], \tag{3}$$

$$\text{Int} = \text{A}[0]\ \exp\left(-B^2/2\right), \tag{4}$$

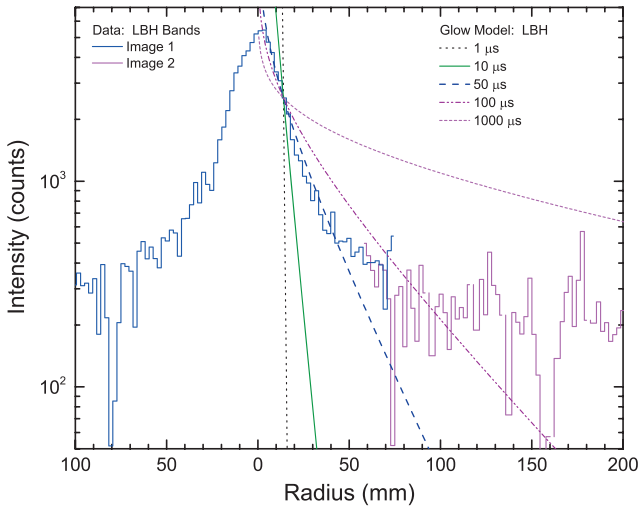

Figure 8. The radial model glow function for an LBH emission point source with an array of lifetimes from 1 μs to 1000 μs shown for Images 1 and 2.

where the output values of a Gaussian-fitting code to intensity data A[0:2] represent the amplitude A[0], the fit center A[1], and the Gaussian width A[2]. We note that the spectral background offset (and sensitivity calibration) was already adjusted prior to fitting the Gaussian. The center value A[1], having maximum intensity, had a fitted value near 0 mm as expected. The Gaussian width of the fitted glow intensity data had a value of 9.86 mm, whereby the FWHM was 23.2 mm, i.e., FWHM = 2 (2 ln 2)$^{1/2}$ × Gaussian width. The values of the three "A" scalars are given in Figure 7. We will construct an LBH glow model that has the same spatial resolution as the IUVS laboratory data set as described by the prompt radiation glow pattern from NI 120.0 nm ("ns" lifetime). The NI (120.0 nm) line profile is broadened by the instrument function arising from the spreading of the electron beam current over the 30 cm path length from mutual electron repulsion over about 50-column pixels (five data points in Figures 6 or 7) of the IUVS FOV producing a spatial FWHM of about 23 mm (see A[2] above) shown in Figure 7. The electron beam is not a perfect infinitesimal line source but has a finite width.

We then convolve the radial model glow function for an LBH emission line source with an array of lifetimes between 1 and 1000 μs in Figure 8 with the kernel of the convolution, *Int*, which is the spatial resolution function of the FOV, shown in Figure 6. We convolve *Int* of the glow model for the glow pattern with two spatial models distinctly representing the glow patterns for direct excitation and cascading. The direct excitation point source models are shown in Figure 8 and then as a starting point we use the asymptotic lifetime values for each process given in Figure 6 that achieve fits to the data near the electron beam from the direct excitation range of 0–40 mm and the asymptotic values for large radii from 100 to 400 mm for cascading. Then using the glow models broadened by these two convolutions that represent separately the two actual observed emission patterns we perform a best fit regression for the glow pattern from a direct excitation lifetime and the glow pattern from a composite cascading lifetime. The multiple linear regression fit returns a two-element column vector of coefficients for each lifetime glow pattern expressed as an exponential with distance. The regression analysis showed a physically meaningful cascade model for the fast component lifetime in the range of ~35–60 μs. We show in Figure 9 the best fit to a combined model fit composed of two lifetimes of the LBH glow data plotted in Figure 6. The best fit model occurs roughly for a direct excitation lifetime of 50 μs with an uncertainty of ~15 μs, and we find ~5000 μs for a composite cascading lifetime.

The final regression model and data match each other well over the entire glow region (0–400 mm). With this data set, we are showing the first conclusive spectroscopic evidence, based on single-scattering conditions, identifying cascading due to the processes $a'^1\Sigma_u^-$ and $w^1\Delta_u \rightarrow a^1\Pi_g$ after direct excitation emission has faded away with radius of the glow pattern about the electron beam. By integrating under the two glow curves and comparing summed intensities over the glow region normalized to unity, we find that direct excitation and cascading occur in the ratio of approximately 0.66: 0.34 at this gas pressure. The ratio was determined by a two-dimensional regression fit using the two lifetimes of 50 μs and 5000 μs. The regression function

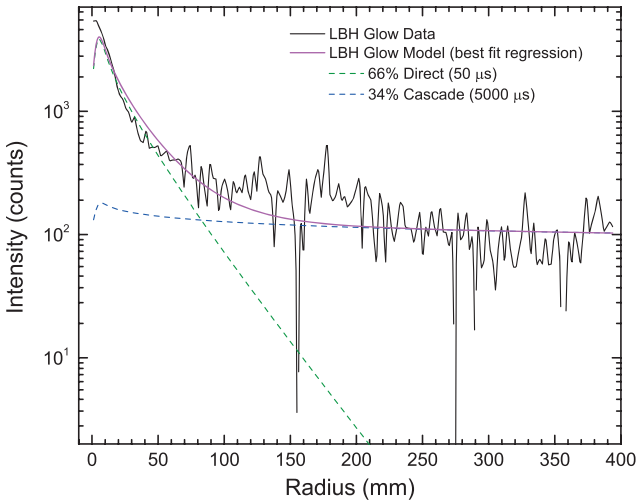

Figure 9. Two comparisons of the models and data for two direct excitation lifetimes: (a) for direct excitation (50 μs) in green and for cascade (5000 μs) in blue. We show the best model regression fit for the two lifetimes in pink. The LBH glow data are in black. Several data dropouts can be found in the FUV LBH data channels. Each data point is 2.21 mm or about a 10-column pixel summation. A glow model composed of two lifetimes that is the best fit of the glow data.

performs a multiple linear regression fit and returns a two-element column vector of coefficients. The lifetimes achieved are within experimental error overlap of the ~55 μs lifetime we estimated from a smaller FOV glow region measurement reported in *Ajello et al.* [2011b], which measured at that time with less *S*/*N* and without modeling the cascading effect to the glow data.

The total emission cross-section (σ^{em}) lower limit can therefore be determined from integrating the measured total intensity glow output between 0 and 400 mm around the electron beam. This area is then compared and normalized to the known cross section of NI 120.0 nm as measured from the glow area of NI 120.0 nm from our experiment (see Figures 6 and 9). Note that the combined statistical and cross-section normalization standard uncertainties was ~13.5%, with the remainder of uncertainty due to systematics such as the relative sensitivity calibration and the glow profile modeling, such that we utilize an estimated root-mean-square 20% accuracy. The excitation and predissociation cross sections can also be estimated, as the following processes indicate.

3. $\sigma^{em} = \sigma^{em}_{dir} + \sigma_{casc}$, where the total LBH emission cross section is the sum of two UV component emission cross sections from process-1, all of the direct excitation σ^{em}_{dir}, and from process-2, most of the σ_{casc} from cascade (IR-cascade + CIET). At our pressure of ~1.5×10^{-5} torr, corresponding to an altitude of ~120–130 km on Earth, the lower limit to the total LBH emission cross section is $\sigma^{em} = 9.71 \times 10^{-18}$ cm^2 at 100 eV. Furthermore, using the 0.66: 0.34 ratio, we can determine the 100 eV LBH cross sections: (1) $\sigma^{em}_{dir} = 0.66 \times 9.71 \times 10^{-18}\,\text{cm}^2 = 6.41 \times 10^{-18}\,\text{cm}^2$ and (2) $\sigma_{casc} = 0.34 \times 9.71 \times 10^{-18}\,\text{cm}^2 = 3.30 \times 10^{-18}\,\text{cm}^2$ as a lower limit at 1.5×10^{-5} torr.
4. Predissociation is an additional process, which occurs on a submicrosecond timescale, without UV radiation for $a^1\Pi_g$ ($v' > 6$) from mainly process-1 (direct excitation), as process-2 populates lower v' levels [*Eastes*, 2000; *Eastes and Dentamaro*, 1996]:

$$e^- + N_2\,(X) \rightarrow N_2^{**} \rightarrow e^- + N + N, \text{ for } a^1\Pi_g\left(v' > 6\right).$$

Here we can calculate σ_{pre} (LBH) at 100 eV from *Ajello and Shemansky* [1985], which indicated a predissociation yield of $\eta = 0.1229$. The predissociation cross section is related to the excitation cross section: $\sigma_{pre} = \eta \times \sigma^{ex}$, where σ^{ex} is the direct excitation cross section of the *a* state. Note that σ^{ex} is given by $\sigma^{ex} = \sigma^{em}_{dir} + \sigma_{fast\_casc} + \sigma_{pre}$. As discussed above, a negligible fast cascade contribution to the $a^1\Pi_g$ state is probable; therefore, $\sigma_{pre} = 8.99 \times 10^{-19}$ cm^2 at 100 eV. This is a lower limit to σ_{pre} since a small portion of slow cascade of process-2 may also contribute to predissociation from the *a* state.

5. The direct excitation cross section of the $a^1\Pi_g$ state at 100 eV is consequently $\sigma^{ex} = \sigma^{em}_{dir} \times 1.14$; therefore, $\sigma^{ex} = 7.37 \times 10$–18 cm^2.

We can compare these results to our recent electron-impact studies in our small chamber where we measured the excitation function of the $a^1\Pi_g$ state for direct excitation without measureable cascading due to a mean-free path of the $a'^1\Sigma_u^-$ excited cascade molecules being greater than the 10 cm chamber characteristic dimension [*Young et al.*, 2010]. Surface collisional deactivation would probably quench these metastable states and negligibly influence the $a^1\Pi_g$ state emission in the experiment of *Young et al.* [2010]. We have also shown that the $c_4'^1\Sigma_u^+$ (0) $-$ $a^1\Pi_g$ cascade is negligible contributing $<$1% of the emission cross section at 100 eV [*Shemansky et al.*, 1995]. The excellent shape of the excitation function found in Young et al., however, is consistent with the excitation cross-section measurement of *Johnson et al.* [2005] for the $a^1\Pi_g$ state. The direct (integral) excitation cross section of *Johnson et al.* [2005], i.e., $\sigma^{ex} = (7.16 \pm 1.29) \times 10^{-18}$ cm^2 at 100 eV, for the $X^1\Sigma_g^+$ (0) $\rightarrow$ $a^1\Pi_g$ (v') transition, adjusted for predissociation (i.e., a 12.29% reduction via FCFs as indicated in Ajello and Shemansky), suggests a direct emission cross section of $\sigma_{dir}^{em} = (6.3 \pm 1.1) \times 10^{-18}$ cm^2 at 100 eV for the entire LBH band system. This direct emission cross section agrees within error bars with the 100 eV value, $\sigma_{dir}^{em} = (5.46 \pm 0.92) \times 10^{-18}$ cm^2, of *Ajello and Shemansky* [1985] as recently summarized in *Ajello et al.* [2011a] and using here the recommended Lyman-alpha emission cross section from Table 7 of *McConkey et al.* [2008] for renormalization. Our present result for the excitation cross section of the $a^1\Pi_g$ state at 100 eV is $\sigma^{ex} = 7.37 \times 10^{-18}$ cm^2, a value very close to the 100 eV excitation cross section result of Ajello and Shemansky of 6.22×10^{-18} cm^2.

The peak excitation cross section near 18 eV can be estimated since the ratio relative to 100 eV is nearly 2.8:1 (peak to 100 eV ratio) [see *Young et al.*, 2010, Table 1]. The peak excitation cross section of the $a^1\Pi_g$ state at 18 eV is $\sigma^{ex} = 2.8 \times (7.37 \times 10^{-18}$ cm$^2) = 2.06 \times 10^{-17}$ cm^2. Therefore, the lower limit to the peak emission cross section at 18 eV is $2.8 \times (\sigma_{dir}^{em}$ (100 eV) + σ_{casc} (100 eV)) $= 2.72 \times 10^{-17}$ cm^2. We also study LBH cross-section results from Image 1 for negative column distances to $-$100 mm in Figures 6 and 7 and deduce a nearly identical result for emission cross sections here using only data for positive z translation by reflecting Image 2 and Image 3 column distances to be negative to $-$400 mm.

Finally, we can compare our lower limit to the cascade emission cross section at 100 eV, a sum of CIET and radiative cascade cross sections from $a'^1\Sigma_u^-$ and $w^1\Delta_u$ to $a^1\Pi_g$, to the summation of the direct excitation cross sections of *Johnson et al.* [2005] of the same two states. We compare our lower limit 100 eV measurement of $\sigma_{casc} = 3.30 \times 10^{-18}$ cm^2 to the Johnson et al. σ^{ex} (a' + w) sum value of approximately $\sigma_{casc} = (1.00 \pm 0.21) \times 10^{-18}$ cm^2 at 100 eV. (We note that *Johnson et al.* [2015] indicates that the excitation cross section of the a' state appears to be significantly larger below the 20 eV value of *Johnson et al.* [2005].) The energy delivered to the $a'^1\Sigma_u^-$ and $w^1\Delta_u$ states would ordinarily both relax to the nearby $a^1\Pi_g$ excited state (as well as to the $X^1\Sigma_g^+$ ground state for the $a'^1\Sigma_u^-$ state, especially a'(0)) in the absence of collisions. The much larger cross section found here indicates how large the contribution of CIET can be to the $a^1\Pi_g$ state total emission cross section, an experimental result that validates the atmospheric models of *Eastes and Dentamaro* [1996] and *Eastes* [2000]. The CIET effect is now verified to be very pronounced in aeronomy in the dayglow region of 120–130 km. Radiation that would ordinarily occur in the IR via the McFarlane I and II bands at high altitudes is now shown to occur as part of the radiative cascade process in the UV from the LBH bands.

4. Conclusion

The LBH emission cross-section ($\sigma^{em} = \sigma_{dir}^{em} + \sigma_{casc}$) lower limit has been determined by measuring the entire glow pattern of the metastable electron-impact-induced emission around an extended length of electron beam from 0 to 400 mm radial distance from the beam axis at 100 eV. The total LBH emission cross section (σ^{em}) is the sum of the cross section for direct excitation of the a state (σ_{dir}^{em}) and that of the cascade contribution (σ_{casc}), i.e., IR-cascade plus CIET from the a' and w states. We find $\sigma^{em} = 9.71 \times 10^{-18}$ cm^2 at 100 eV. In this experiment at a pressure of 1.5×10^{-5} torr, direct excitation of the a state accounts for ~66% of the LBH emission ($\sigma_{dir}^{em} = 6.41 \times 10^{-18}$ cm^2) with cascade accounting for ~34% ($\sigma_{casc} = 3.30 \times 10^{-18}$ cm^2) of the glow pattern up to 400 mm radial distance. The contribution to the glow pattern for lines of sight beyond 400 mm in this experiment depends on the optically allowed $a' \leftrightarrow a$ and $w \leftrightarrow a$ radiative lifetimes for radiative cascade and CIET contributions. We find the lifetime for the optically forbidden $a^1\Pi_g$ state to be ~50 ± 15 μs, with the mean lifetime for cascade from the $a'^1\Sigma_u^-$ and $w^1\Delta_u$ states, by radiative and collision-induced electronic transitions, to be about 5 ms.

Past fluorescence cross-section laboratory studies [e.g., see *Young et al.*, 2010, Figure 4] investigated pressure influences on the LBH emission but had smaller FOVs that corresponded to our on-center results (i.e., a subset of Image 1). Our future laboratory work will study the vibrational intensities of the v' progressions of the LBH band system with radial distance from the electron beam and compare the vibrational progression intensities to Table 4 of *Eastes and Dentamaro* [1996]. The CIET effect is now verified to be very pronounced in aeronomy in Earth's dayglow region of 120–130 km and probably Titan's extended and thick upper atmosphere dayglow and nightglow regions of 500−1400 km [*Ajello et al.*, 2012; *Stevens et al.*, 2011]. Radiation that would ordinarily occur in the IR via the McFarlane I and II bands at high altitudes is now shown to occur as part of the radiative cascade process in the UV from the LBH bands. Preliminary spectral results from the present study show that the ($v' = 0$, v″) vibrational intensities are the most enhanced vibrational progression, in agreement with Eastes and Dentamaro, when comparing Image 2 and Image 3 with respect to Image 1 of the present work.

Acknowledgments
This work was performed at the Laboratory for Atmospheric and Space Physics (LASP), University of Colorado (CU), and the Jet Propulsion Laboratory (JPL), California Institute of Technology (Caltech), under a contract with the National Aeronautics and Space Administration (NASA). We gratefully acknowledge financial support through NASA's Cassini Data Analysis Program, the Heliophysics HTIDES and Geospace Science programs, the National Science Foundation Aeronomy Program Office, and the Mars Data Analysis Program Office. We thank David Hall for technical support and Nick Schneider, Bruce Jakosky, and the MAVEN team for usage of the IUVS optical-engineering unit. The data used are listed in the references; otherwise, please e-mail the corresponding author for data tables.
Copyright 2017 California Institute of Technology. Government sponsorship is acknowledged.

References

Ajello, J., V. Vattipalle, and G. Osinski (2002), UV spectroscopy by electron impact for planetary astronomy and astrophysics, in *Current Developments in Atomic, Molecular, and Chemical Physics with Applications*, edited by M. Mohan, pp. 143–151, Kluwer Acad., /Plenum Publ., New York.

Ajello, J. M. (1970), Emission cross sections of N_2 in the vacuum ultraviolet by electron impact, *J. Chem. Phys.*, *53*, 1156.

Ajello, J. M., and D. E. Shemansky (1985), A re-examination of important N_2 cross sections by electron impact with application to the dayglow: The Lyman-Birge Hopfield band system and NI (119.99 nm), *J. Geophys. Res.*, *90*, 9845–9861, doi:10.1029/JA090iA10p09845.

Ajello, J. M., et al. (1988), A simple ultraviolet calibration source with reference spectra and its use with the Galileo Orbiter Ultraviolet Spectrometer, *Appl. Opt.*, *27*, 890.

Ajello, J. M., G. K. James, B. O. Franklin, and D. E. Shemansky (1989), Medium-resolution studies of extreme ultraviolet emission from N_2 by electron impact: Vibrational perturbations and cross sections of the $c'_4\ ^1\Sigma_u^+$ and $b'\ ^1\Sigma_u^+$ states, *Phys. Rev. A.*, *40*, 3524–3556.

Ajello, J. M., D. Shemansky, W. Pryor, A. Stewart, K. Simmons, T. Majeed, H. Waite, and G. Gladstone (2001), Spectroscopic evidence for high altitude aurora from Galileo extreme ultraviolet and Hopkins ultraviolet telescope observations, *Icarus*, *152*, 151–171.

Ajello, J. M., M. H. Stevens, I. Stewart, K. Larsen, L. Esposito, J. Colwell, W. McClintock, G. Holsclaw, J. Gustin, and W. Pryor (2007), Titan airglow spectra from Cassini Ultraviolet Imaging Spectrograph (UVIS): EUV analysis, *Geophys. Res. Lett.*, *34*, L24204, doi:10.1029/2007GL031555.

Ajello, J. M., J. Gustin, I. Stewart, K. Larsen, L. Esposito, W. Pryor, W. McClintock, M. H. Stevens, C. P. Malone, and D. Dziczek (2008), Titan airglow spectra from Cassini Ultraviolet Imaging Spectrograph: FUV analysis, *Geophys. Res. Lett.*, *35*, L06102, doi:10.1029/2007GL032315.

Ajello, J. M., R. S. Mangina, and R. R. Meier (2011a), UV molecular spectroscopy from electron impact for applications to planetary atmospheres and astrophysics, in *Charged Particle and Photon Interactions With Matter: Recent Advances, Applications, and Interfaces*, edited by Y. Hatano, Y. Katsumura, and A. Mozumder, chap. 28, p. 761, CRC Press, Boca Raton, Fla.

Ajello, J. M., R. Mangina, and D. Strickland (2011b), Laboratory studies of UV emissions from proton impact on N_2 for aurora analysis: The Lyman-Birge-Hopfield band system, *J. Geophys. Res.*, *116*, A00K03, doi:10.1029/2010JA016103.

Ajello, J. M., R. West, M. Stevens, K. Larsen, A. I. Stewart, L. W. Esposito, W. E. McClintock, G. M. Holsclaw, and E. T. Bradley (2012), Cassini UVIS observations of Titan nightglow spectra, *J. Geophys. Res.*, *117*, A12315, doi:10.1029/2012JA017888.

Aksnes, A., R. Eastes, S. Budzien, and K. Dymond (2006), Neutral temperatures in the lower thermosphere from N_2 Lyman-Birge-Hopfield (LBH) band profiles, *Geophys. Res. Lett.*, *33*, L15103, doi:10.1029/2006GL026255.

Aksnes, A., R. Eastes, S. Budzien, and K. Dymond (2007), Dependence of neutral temperatures in the lower thermosphere on geomagnetic activity, *J. Geophys. Res.*, *112*, A06302, doi:10.1029/2006JA01221.

Allen, J. S., and C. C. Lin (1989), Electron-impact excitation of the vibrational levels of the cc electronic state of the nitrogen molecule, *Phys. Rev. A*, *39*, 383–386.

Allen, J. S., S. Chung, and C. C. Lin (1990), Electron-impact excitation of the xx, yy, and o3 Rydberg electronic states of the nitrogen molecule, *Phys. Rev. A*, *41*, 1324–1334.

Brunger, M. J., and P. J. O. Teubner (1990), Differential cross sections for electron-impact excitation of the electronic states of N_2, *Phys. Rev. A*, *41*, 1413–1426.

Cartwright, D. (1978), Vibrational populations of the excited states of N_2 under auroral conditions, *J. Geophys. Res.*, *83*, 517–531, doi:10.1029/JA083iA02p00517.

Cartwright, D. C., A. Chutjian, S. Trajmar, and W. Williams (1977a), Electron impact excitation of the electronic states of N2, I, differential cross sections at incident energies from 10 to 50 eV, *Phys. Rev. A*, *16*, 1013–1040.

Cartwright, D. C., S. Trajmar, A. Chutjian, and W. Williams (1977b), Electron impact excitation of the electronic states of N2, II, integral cross sections at incident energies from 10 to 50 eV, *Phys. Rev. A*, *16*, 1041–1051.

Casassa, M. P., and M. F. Golde (1979), Vacuum UV emission by electronically-excited N_2: The radiative lifetime of the N2 ($a'^1\Sigma_u^-$) state, *Chem. Phys. Let.*, *60*, 281–285.

Dahl, F., and J. Oddershede (1986), Radiative lifetime of the forbidden $a^1\Pi_g \leftarrow X^1\Sigma_g^+$ transition of N_2, *J. Phys. Scr.*, *33*, 135.

Eastes, R., et al. (2015), Imaging the boundary between Earth and space—A preview of space weather data from the Global-scale Observations of the Limb and Disk (GOLD) mission, 2015 Space Weather Week, 13-17 April, abstract and invited presentation.

Eastes, R. W. (2000), Modeling the N_2 Lyman-Birge-Hopfield bands in the dayglow: Including radiative and collisional cascading between the singlet states, *J. Geophys. Res.*, *105*, 18,557–18,573, doi:10.1029/1999JA000378.

Eastes, R. W., and A. V. Dentamaro (1996), Collision-induced transitions between the $a^1\Pi_g$, $a'^1\Sigma_u^-$, $w^1\Delta_g$ states of N_2: Can they affect auroral N_2 Lyman-Birge-Hopfiled band emissions?, *J. Geophys. Res.*, *101*, 26,931–26,940, doi:10.1029/96JA01636.

Eastes, R. W., D. J. Murray, A. Aksnes, S. A. Budzien, R. E. Daniell, and A. Krywonos (2011), Modeled and observed N_2 Lyman-Birge-Hopfield band emissions: A comparison, *J. Geophys. Res.*, *116*, A12308, doi:10.1029/2010JA016417.

Eastes, R. W., et al. (2008), Global-scale Observations of the Limb and Disk (GOLD): New observing capabilities for the Ionosphere-Thermosphere, in *Midlatitude Ionospheric Dynamics and Disturbances*, *Geophys. Monogr. Ser.*, vol. 181, edited by P. M. Kintner Jr. et al., pp. 319–326, AGU, Washington, D. C.

Esposito, L., et al. (2004), The Cassini Ultraviolet Imaging Spectrograph investigation, *Space Sci. Rev.*, *115*, 299.

Filippelli, A. R., S. Chung, and C. C. Lin (1984), Electron-impact excitation of the DD and cc Rydberg states of N_2, *Phys. Rev. A*, *29*, 1709–1728.
Filippelli, A. R., C. C. Lin, L. W. Anderson, and J. W. McConkey (1994), Measuring electron-impact excitation cross sections, *Adv. At. Mol. Opt. Phys.*, *33*, 1–62.
Gilmore, F. R., R. R. Laher, and P. J. Espy (1992), Franck-Condon factors, r-centroids, electronic transition moments, and Einstein coefficients for many nitrogen and oxygen band systems, *J. Chem. Phys. Ref. Data*, *21*(5), 1005.
Harting, E., and F. H. Read (1976), *Electrostatic Lenses*, p. 322, Elsevier Sci. Co., New York.
Holland, R. F. (1969), Excitation of nitrogen by electrons: The Lyman-Birge-Hopfield system of N_2, *J. Chem. Phys.*, *51*, 3940.
Itikawa, Y. (2006), Cross sections for electron collisions with nitrogen molecules, *J. Chem. Phys. Ref. Data*, *35*(1), 31–53.
Itikawa, Y., et al. (1986), Cross sections for collisions of electrons and photons with nitrogen molecules, *J. Chem. Phys. Ref. Data*, *15*, 985–1010.
Johnson, P. V., C. P. Malone, I. Kanik, K. Tran, and M. A. Khakoo (2005), Integral cross-sections for the direct excitation of the a $^3\Sigma_u^+$, $B^3\Pi_g$, $W^3\Delta_u$, $B'\,^3\Sigma_u^-$, $a'^1\Sigma_u^-$, $a^1\Pi_g$, $w^1\Delta_u$, and $C^3\Pi_u$ electronic states in N_2 by electron impact, *J. Geophys. Res.*, *110*, A11311, doi:10.1029/2005JA011295.
Johnson, P. V., X. Liu, C. P. Malone, J. D. Hein, and M. A. Khakoo (2015), Excitation of atmospheric species by electron impact, 68th Gaseous Electronics Conference (GEC), Honolulu, Hawaii, Oct. 12–16, 2015, (Bulletin of the APS, 60 (9), Abstract BAPS.2015.GEC.LW1.3).
Kanik, I., L. W. Beegle, J. M. Ajello, and S. C. Solomon (2000), Electron-impact excitation/emission and photoabsorption cross sections important in the terrestrial airglow and auroral analysis of rocket and satellite observations, *Phys. Chem. Earth Part C*, *25*, 573.
Kanik, I. Noren, C., O. Makarov, P. Vatti Palle, J. Ajello and D. Shemansky (2003), Electron impact dissociative excitation of O_2. II. Absolute emission cross sections of OI(130.4 nm) and OI(135.6 nm), *J. Geophys. Res.*, *108*(E11), 5126, doi:10.1029/2000JE001423.
Kedzierski, W., and J. W. McConkey (2016a), Use of solid N_2 surfaces in metastable particle detection, *J. Chem. Phys.*, *145* 044313.
Kedzierski, W., and J. W. McConkey (2016b), Use of solid N_2 surfaces in metastable particle detection, *Rev. Sci. Instrum.*, *87* 123110.
Kil, H., Y.-S. Kwak, L. J. Paxton, R. R. Meier, and Y. Zhang (2011), O and N_2 disturbances in the *F* region during the 20 November 2003 storm seen from TIMED/GUVI, *J. Geophys. Res.*, *116*, A02314, doi:10.1029/2010JA016227.
Khakoo, M. A., C. P. Malone, P. V. Johnson, B. R. Lewis, R. Laher, S. Wang, V. Swaminathan, D. Nuyujukian, and I. Kanik (2008), Electron impact excitation of $X^1\Sigma_g^+$ (v''=0) to the $a''^1\Sigma_g^+$, $b^1\Pi_u$, $c_3{}^1\Pi_u$, $o_3{}^1\Pi_u$, $b'^1\Sigma_u^+$, $c'_4{}^1\Sigma_u^+$, $G^3\Pi_u$, and $F^3\Pi_u$ states of molecular nitrogen, *Phys. Rev. A: At. Mol. Opt. Phys.*, *77*, 012704.
Knight, H. K., D. J. Strickland, J. H. Hecht, P. R. Strus, D. Morrison, L. J. Paxton, F. J. Rich, and D. S. Evans (2008), Evidence for significantly greater N_2 LBH emission efficiencies in proton vs electron Aurora based on analysis of coincident DMSP SSUSI and SSJ.5 data, *J. Geophys. Res.*, *113*, A04305, doi:10.1029/2007JA012728.
Krywonos, D., J. Murray, R. W. Eastes, A. Aksnes, S. A. Budzien, and R. E. Daniell (2012), Remote sensing of neutral temperatures in the Earth's thermosphere using the Lyman-Birge-Hopfield bands of N_2: Comparisons with satellite drag data, *J. Geophys. Res.*, *117*, A09311, doi:10.1029/2011JA017226.
Laher, R. R. (1999), Spectroscopy research. [Available at http://spider.ipac.caltech.edu/staff/laher/fluordir/fluorindex.html (Accessed 25 April 2017)].
Laher, R. R., and F. R. Gilmore (1991), Improved fits for the vibrational and rotational constants of many states of nitrogen and oxygen, *J. Chem. Phys. Ref. Data*, *20*(4), 685.
Liu, X., S. Ahmed, R. Multari, G. James, and J. M. Ajello (1995), High resolution electron impact study of the FUV emission spectrum of molecular hydrogen, *Ap. J. Supp.*, *101*, 001.
Lofthus, A., and P. H. Krupenie (1977), The spectrum of molecular nitrogen, *J. Phys. Chem. Ref. Data*, *6*, 113–307.
Lummerzheim, D., and M. Galand (2001), The profile of the hydrogen H_β emission line in proton aurora, *J. Geophys. Res.*, *106*, 23–32, doi:10.1029/2000JA002014.
Makarov, O., I. Kanik, J. Ajello and C. Noren (2003), Electronic impact dissociative excitation of O_2. I. Kinetic energy distributions of fast oxygen atoms, *J. Geophys. Res.*, *108*(E11), 5125, doi:10.1029/2000JE001422.
Malone, C. P., P. V. Johnson, J. W. McConkey, J. M. Ajello, and I. Kanik (2008), Dissociative excitation of N_2O by electron impact, *J. Phys. B: At. Mol. Opt. Phys.*, *41*, doi:10.1088/0953-4075/41/9/095201.
Malone, C. P., P. V. Johnson, I. Kanik, B. Ajdari, and M. A. Khakoo (2009a), Electron impact excitation of molecular nitrogen. I. Excitation of the $C^3\Pi_u$, $E^3\Sigma_g^+$, and $a''^1\Sigma_g^+$ states, *Phys. Rev. A: At. Mol. Opt. Phys.*, *79*, 032704.
Malone, C. P., P. V. Johnson, I. Kanik, B. Ajdari, S. S. Rahman, S. S. Bata, A. Emigh, and M. A. Khakoo (2009b), Electron impact excitation of molecular nitrogen. II. Vibrationally-resolved excitation of the $C^3\Pi_u$ (v') state, *Phys. Rev. A: At. Mol. Opt. Phys.*, *79*, 032705.
Malone, C. P., P. V. Johnson, J. A. Young, B. Ajdari, M. A. Khakoo, X. Liu, and I. Kanik (2009c), Integral cross sections for the electron-impact excitation of the $C^3\Pi_u$, $E^3\Sigma_g^+$, and $a''^1\Sigma_g^+$ states of N_2, *J. Phys. B: At. Mol. Opt. Phys.*, *42*, 225202.
Malone, C. P., P. V. Johnson, X. Liu, B. Ajdari, I. Kanik, and M. A. Khakoo (2012), Integral cross sections for the electron impact excitation of the $b^1\Pi_u$, $c_3{}^1\Pi_u$, $o_3{}^1\Pi_u$, $b'^1\Sigma_u^+$, $c'_4{}^1\Sigma_u^+$, $G^3\Pi_u$, and $F^3\Pi_u$ states of N_2, *Phys. Rev. A: At. Mol. Opt. Phys.*, *85*, 062704.
Malone, C. P., J. M. Ajello, A. C. Hoskins, W. E. McClintock, and P. V. Johnson (2015), Electron impact of CO, CO_2, and N_2 using the MAVEN IUVS flight spare, 68th Gaseous Electronics Conference (GEC), Honolulu, Hawaii, Oct. 12–16. (Bulletin of the APS, 60 (9), Abstract BAPS.2015.GEC.GT1.8).
Mannucci, A. J. B., T. Tsurutani, S. C. Solomon, O. P. Verkhoglyadova, and J. P. Thayer (2012), How do coronal hole storms affect the upper atmosphere?, *Eos Trans. AGU*, *93*(8), 77, doi:10.1029/2012EO080002.
Marinelli, W. J., W. J. Kessler, B. D. Green, and W. A. M. Blumberg (1989), The radiative lifetime of N_2 ($a^1\Pi_g$, v = 0-2), *J. Chem Phys.*, *91*, 701.
McClintock, W. E., N. Schneider, G. Hosclaw, J. T. Clarke, A. Hospkinms, I. Stewart, F. Montmessin, R. Yelle, and J. Deighan (2015), The Imaging Ultraviolet Spectrograph (IUVS) for the MAVEN mission, *Space Sci. Rev.*, doi:10.1007/s11214-014-0098-7.
McConkey, J. W., C. P. Malone, P. V. Johnson, I. Kanik, C. E. Winstead, and V. McKoy (2008), Electron impact dissociation of oxygen-containing molecules — A critical review, *Phys. Rep.*, *466*, 103, doi:10.1016/j.physrep.2008.05.001.
Meier, R. R. (1991), Ultraviolet spectroscopy and remote sensing of the upper atmosphere, *Space Sci. Rev.*, *58*, 1–185.
Meier, R. R., G. Crowley, D. J. Strickland, A. B. Christensen, L. J. Paxton, D. Morrison, and C. L. Hackert (2005), First look at the November 20, 2003 super storm with TIMED/GUVI, *J. Geophys. Res.*, *110*, A09S41, doi:10.1029/2004JA010990.
Meier, R. R., et al. (2015), Remote sensing of Earth's limb by TIMED/GUVI: Retrieval of thermospheric composition and temperature, *Earth Space Sci.*, 1–37, doi:10.1002/2014EA000035.
Noren, C., I. Kanik, J. M. Ajello, P. McCartney, O. Makarov, W. McClintock, and V. Drake (2001), Emission cross section of O I (135.6 nm) at 100 eV resulting from electron-impact dissociative excitation of O_2, *Geophys. Res. Lett.*, *28*, 1379–1382, doi:10.1029/2000GL012577.
Paxton, L. J., et al. (1999), Global Ultraviolet Imager (GUVI): Measuring composition and energy inputs for the NASA Thermosphere Ionosphere Mesosphere Energetics and Dynamics (TIMED) mission, in *Optical Spectroscopic Techniques and Instrumentation for Atmospheric and Space Research III*, vol. 3756, edited by A. M. Larar, pp. 265–276, Int. Soc. for Opt. Eng., Bellingham, Wash., doi:10.1117/12.366380.

Shemansky, D. E., I. Kanik, and J. M. Ajello (1995), Fine structure branching in N_2 $c'4^1\Sigma_u^+$ (0), *Ap. J.*, *452*, 480.
Stevens, M., et al. (2011), The production of Titan's ultraviolet nitrogen airglow, *J. Geophys. Res.*, *116*, A05304, doi:10.1029/2010JA016284.
Stevens, M. H., et al. (2015), N_2 in the upper atmosphere of Mars observed by IUVS on MAVEN, *Geophys. Res. Lett.*, *42*, 9050–9056, doi:10.1002/2015GL065319.
Strickland, D. J., J. E. Bishop, J. S. Evans, T. Majeed, P. M. Shen, R. J. Cox, R. Link, and R. E. Huffman (1999), Atmospheric Ultraviolet Radiance Integrated Code (AURIC): Theory, software architecture, inputs, and selected results, *J. Quant. Spectrosc. Radiat. Transfer*, *62*, 689.
Tilford, S. G., and W. M. Benesch (1976), Absorption oscillator strengths for the $a'^1\Sigma_u^- \rightarrow X^1\Sigma_g^+$ and $a'^1\Sigma_u^-$ and $w^1\Delta_u \rightarrow X^1\Sigma_g^+$ transitions of molecular nitrogen, *J. Chem. Phys.*, *64*, 3370–3374.
Vanhamäki, H., and O. Amm (2011), Analysis of ionospheric electrodynamic parameters on mesoscales—A review of selected techniques using data from ground-based observation networks and satellites, *Ann. Geophys.*, *29*, 467–491.
Wilkinson, P. G., and R. S. Mulliken (1959), Forbidden band systems in nitrogen. II. The $a'^1\Sigma_u^-$-$X^1\Sigma_g^+$ system in absorption, *J. Chem. Phys.*, *31*, 674–679.
Young, J. A., C. P. Malone, P. V. Johnson, J. M. Ajello, X. Liu, and I. Kanik (2010), Lyman-Birge-Hopfield emissions from electron impact excited N_2, *J. Phys. B: At. Mol. Opt. Phys.*, *43*, doi:10.1088/0953-4075/43/13/135201.